DEVELOPMENT OF MODEL PREDICTIVE CONTROL FOR MAGNETIC LEVITATION SYSTEMS

Abstract

The study of Magnetic Levitation systems (Maglev) has gained significant attention due to their minimal friction and energy-efficient attributes, which are deemed crucial factors. This paper introduces a novel magnetic levitation system implemented through the Simulink environment. The dynamics of Maglev exhibit nonlinearity and high instability, which renders the task of devising an appropriate control algorithm even more challenging. The main goal of this research is to control the position of a ferromagnetic ball within the airspace of the nonlinear system. In this investigation, the suggested controller is formulated based on the linear predictive model, derived by approximating the system's behavior around a known operational point. The efficacy of the designed control approach is validated through simulation levitation model. The performance of the suggested controller is evaluated in comparison to an existing PID control method [1], and it demonstrates superior results.

Keywords: Magnetic Levitation systems, friction, maglev, linear.

Author

Lakshmi Dutta
University Science Instrumentation Centre
North Bengal University
Siliguri, West Bengal India.

I. INTRODUCTION

Magnetic levitation systems hold practical significance across diverse engineering applications. Examples include their utilization in high-speed maglev passenger trains, bearings designed for frictionless movement, elevating wind tunnel models, isolating vibrations in delicate machinery, suspending molten metal within induction furnaces, and raising metal slabs during manufacturing processes. Depending on the origin of levitation forces, maglev systems can be categorized as either attractive or repulsive setups. Typically, these types of systems exhibit instability when operated in open-loop configurations and are characterized by complex nonlinear differential equations, which introduce added challenges in controlling them. As a result, a crucial attempt involves the development of high-performance predictive controllers aimed at effectively managing the position of the levitated object.

Recently, numerous studies have emerged in the literature concerning the control of magnetic levitation systems. These conventional practices involved linearizing the magnetic levitation system at the equilibrium point using Taylor-series expansion. Subsequently, controllers like the proportional- integral-derivative (PID) [2] and linear-quadratic regulator (LQR) [3] were designed. However, this linearization approximation method led to reduced robustness in magnetic levitation control systems as certain nonlinear terms were overlooked. The feedback linearization technique has found application in devising control strategies for magnetic levitation systems [4], [5]. This approach aimed to improve upon the drawbacks of the approximation linearization method. The subsequent adoption of the backstepping technique in controller design [6], [7] marked a further step in this direction. In recent years, more advanced control techniques have been designed to man- age in Maglev system. These include robust-control, adaptive- control, conventional control, or various combinations of these techniques. Authors in [8] introduced a robust controller for a nonlinear system (Maglev), enhancing robustness against parametric uncertainties and unwanted disturbances. Similarly, [9] put forth an advance disturbance observer based controller to improved the forces involved in levitating and stabilizing the Maglev vehicle system. In the reference [10], the authors utilized an adaptive sliding mode control (SMC) law in combination with a magnetic flux observer for Maglev. This control strategy was applied to handle model uncertainties and external disturbances, enhancing the system's robustness and stability. However, the challenge of chattering remained a significant hurdle in SMC application. Subsequent efforts explored intelligent control methods to tackle the intricate nonlinearity of magnetic levitation systems. In the reference [11], a novel fuzzy controller was presented for the levitation system. This controller was built upon the Takagi-Sugeno fuzzy model and incorporated a H_∞ control law. The aim was to improve the system's robustness against parameter perturbations and external disturbances, enhancing its overall performance and stability. Building on this, an improved approach using a parallel-distributed compensation scheme was presented [11], albeit with the challenge of establishing stable fuzzy logic rules. In [12], a fuzzy neural network (NN) was employed to emulate an adaptive observer, forming a control framework for hybrid permanent magnet and electromagnet Maglev transportation systems. This approach exhibited excel- lent performance due to the model-free nature of NN. How- ever, the methods mentioned earlier have certain limitations when it comes to addressing constraints in the context of magnetic levitation systems. These constraints pertain to real- time requirements that ensure reliability [13], [14]. In the case of Maglev

trains, it's essential to consider state constraints such as the air gap, vertical-velocity, and acceleration to meet the reliability criteria for aspects like ride comfort, energy efficiency, and system implementation [15].

Model predictive controller (MPC) is a widely adopted approach in industrial process control that excels in handling both control and state constraints explicitly and optimally [14]. Model Predictive Control (MPC) encompasses solving an optimal control problem with a finite horizon that shifts as time progresses [16]. This involves solving the control sequence for the current situation online during each sampling moment, with only the initial control element of the sequence being employed [17]. Additionally, the present state variables of the process are utilized as the starting point for the optimization problem. MPC methods do have a computational cost, which results from the ongoing need for online optimisation, which is one of its limitations. This is a significant barrier for fast-response systems and turns into a major problem for MPC applications. In recent times, researchers have effectively employed MPC across various domains. These include its application in robotics [18], energy-efficient control of twin rotor MIMO system [19], electrical vehicles [20] and power system etc. The MPC approach has also been extended to encompass magnetic levitation ball systems. In the paper [21], a robust MPC was introduced for a second-order maglev system. This controller was designed to handle both input and output constraints, ensuring the stable and constrained operation of the system. In this study, the model uncertainties are effectively addressed through the utilization of the linear matrix inequalities (LMI) technique. In the work presented in [22], the authors developed an MPC controller for the maglev system using a pre-identified state-dependent model based on the autoregressive with exogenous variables (ARX) approach, which was established through a set of radial basis function neural networks (RBF NNs). Further, in [23], [24] the authors introduced an explicit model predictive controller (EMPC) for the magnetic levitation system. They strategically moved the optimization process offline, aiming to improve real-time performance while considering both input and output constraints. They accounted for both input and output constraints for a piece-wise affine (PWA) linear system. Moreover, authors in [25] have introduced a nonlinear MPC (NMPC) approach to the maglev system. This approach aimed to achieve high control performance by accurately predicting the nonlinear system behavior. Nevertheless, the design complexity associated with NMPC posed computational challenges greater than those of linear MPC schemes, thus restricting the consideration of control constraints to maintain real-time feasibility.

The primary aim of this research is to create a linear model predictive control (MPC) technique designed specifically for a Maglev system. The proposed control approach has been evaluated through simulations conducted on magnetic levitation systems, employing three different input signals. The simulation results demonstrate that the proposed control algorithm exhibits superior tracking performance compared to the existing control technique [1].

II. SYSTEM MODELING

Fig.1 depicts a schematic representation of a Maglev system and the physical parameters are detailed in TABLE I. The various mechanical parts and its motions can be anticipated from this schematic diagram. The magnetic force balances the gravitational force exerted on the ferromagnetic ball during the operation of the Maglev system. By altering the

input current, the magnetic force of the Maglev may be changed. As a result, in the Maglev model, the magnetic force corresponds to the square of the electromagnetic coil current. With the aid of the controller, the system receives input from the coil current to regulate the location of the iron ball. This force is subsequently balanced within the airspace to meet the specified requirements.

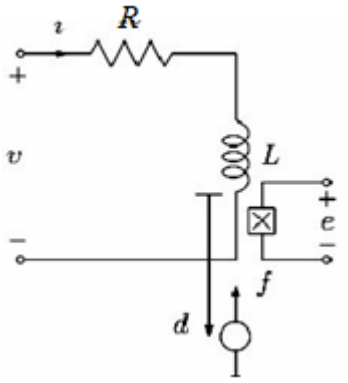

Figure 1: Schematic diagram of the Maglev system

Table I: Maglev system parameters

Parameter	Value	Unit
β	5.64×10^{-4}	$V\,m^2$
γ	0.31	V/A
α	2.48	V
i_0	1	A
d_0	20	mm
C	2.4×10^{-6}	Kgm^5/s^2
R	2	Ohm
L	15×10^{-3}	H
$m = \frac{M}{4}$	0.02985	Kg

1. **State Space Model:** The design and components of the magnetic levitation system will be described in this section. The system consists of four electromagnets that act as actuators to apply magnetic forces for accurate position control. Additionally, there are four Hall Effect sensors integrated into the system to monitor the position of the levitating plate. The setup also consists of a sturdy square plate featuring four permanent magnets, one at each corner. The electromagnets are 2 ohm internal-resistance solenoid coils with a 15 mH rating. Linear radio- metric Hall Effect sensors with a 50 V/T are used in Hall effects experiments. The neodymium *N* 52 disc magnets have a 12.70 mm diameter and a 6.35 mm thickness, and they are used as permanent magnets. The electromagnetic levitation system model is illustrated in Fig.1, where *R* represents the coil's resistance, *L* signifies its inductance, *v* corresponds to the voltage across the electromagnet, *i* represents the current flowing through it, *m* indicates the mass of the levitating system, *g* denotes the gravitational acceleration, *d* signifies the vertical position of the ball measured from the bottom, f denotes the force on the levitating system generated by the electromagnet, and e stands for the voltage across the Hall effect

sensor. The force produced by the electromagnet is mathematically expressed as:

$$F_{mag} = C \frac{i(t)}{d^3} \quad (1)$$

where d is the vertical position and C is a turn constant. From (1) we got

$$M\ddot{d} = mg - C\frac{i(t)}{d^3} \quad (2)$$

where m is the mass of the levitating magnet and g is the gravity of acceleration. The power supply and electromagnetic coil can be related electrically by using the following expression:

$$v(t) = R.i(t) + L\frac{di}{dt} \quad (3)$$

where R and L represent the resistance and inductance of the electromagnet, respectively. Now, let's consider the following perturbations concerning changes in these parameters.

$$i(t) = i_0 + \Delta i(t) \quad (4)$$
$$d(t) = d_0 + \Delta d(t) \quad (5)$$
$$v(t) = v_0 + \Delta v(t) \quad (6)$$

where the voltage needed to suspend the levitating plate at do is called vo. Under this perturbation, it is possible to linearize the dynamics (2) and (3) around an operational point (i_0; d_0; v_0) as

$$m\ddot{\Delta}d = \left(\frac{3Ci_0}{d_0^4}\right)\Delta d - \left(\frac{C}{d_0^3}\right)\Delta i \quad (7)$$
$$\dot{\Delta}i = \left(\frac{R}{L}\right)\Delta i - \left(\frac{1}{L}\right)\Delta v \quad (8)$$

The transfer function from Δv to Δd is obtained by removing Δi in equation (8) and using Laplace transforms as

$$\frac{\Delta D(s)}{\Delta V(s)} = \frac{-\frac{g^R}{v_0}}{(Ls+R)(s^2 - \frac{3Ci_0}{md_0^4})} \quad (9)$$

where ΔV (s) and ΔD(s) represent the Laplace transforms of Δv(t) and Δd(t), respectively. The output voltage of the Hall sensor is as follows.

$$e(t) = \alpha + \frac{\beta}{d^2} + \gamma i(t) \quad (10)$$

where α, β, γ are constant sensor parameters. Linearizing (10) around e(t) = e0 + Δe yields

$$e(t) = \frac{2\beta}{d^3}\Delta d + \gamma \Delta i \tag{11}$$

where Δe is the sensor voltage. We can determine the relationship between the electromagnet voltage perturbation ΔV (s) and the sensor voltage perturbation ΔE(s) by applying the Laplace transform to equation (11) and utilizing I(s) = ΔV (s)/(Ls + R) from equation (3) and the representation in equation (9). This relationship is expressed as follows:

$$\frac{\Delta E(s)}{\Delta V(s)} = \frac{\gamma(s^2 - \frac{3Ci_0}{md_0^4}) + (\frac{2\beta RC}{md_0^6})}{(Ls+R)(s^2 - \frac{3Ci_0}{md_0^4})} \tag{12}$$

After taking the second derivative of equation (7) and the first derivative of equation (8), equation (12) can be transformed into a state-space representation. Consequently, the linearized model described in equation (12) can be represented in statespace form as follows:

$$\begin{bmatrix} \dot{x}_1 \\ \dot{x}_2 \\ \dot{x}_3 \end{bmatrix} = \begin{bmatrix} 0 & 1 & 0 \\ 3\frac{C}{m}\frac{i_0}{d_0^4} & 0 & -\frac{C}{m}\frac{1}{d_0^3} \\ 0 & 0 & -\frac{R}{L} \end{bmatrix} \begin{bmatrix} x_1 \\ x_2 \\ x_3 \end{bmatrix} + \begin{bmatrix} 0 \\ 0 \\ \frac{1}{L} \end{bmatrix} u \tag{13}$$

The measured system output (y) can be obtained by simplifying Equation (11), where (Δe = y, Δd = x1, and Δi = x3).

$$y = \begin{bmatrix} -2\frac{\beta}{d^3} & 0 & \gamma \end{bmatrix} \begin{bmatrix} x_1 \\ x_2 \\ x_3 \end{bmatrix} \tag{14}$$

By substituting system parameters in TABLE I into (12) we get

$$G(s)H(s) = \frac{20.66s^2 + 61803}{s^3 + 132.5s^2 - 1471s - 194900} \tag{15}$$

Here are the numerical values of the state space equations:

$$\begin{bmatrix} \dot{x}_1 \\ \dot{x}_2 \\ \dot{x}_3 \end{bmatrix} = \begin{bmatrix} 0 & 1 & 0 \\ 1471 & 0 & -9.81 \\ 0 & 0 & -133 \end{bmatrix} \begin{bmatrix} x_1 \\ x_2 \\ x_3 \end{bmatrix} + \begin{bmatrix} 0 \\ 0 \\ 66.66 \end{bmatrix} u \tag{16}$$

$$y = \begin{bmatrix} -144 & 0 & 0.31 \end{bmatrix} \begin{bmatrix} x_1 \\ x_2 \\ x_3 \end{bmatrix} \tag{17}$$

III. CONTROL DESIGN

1. **PID Control Design:** This section aims to illustrate the fundamental structure of a PID controller in the context of closed-loop control for the Maglev system, with the objective of maintaining the ball's position at the desired level. In order to explain the PID controller for a levitation system, it's necessary to possess an appropriate mathematical model of the Maglev system. It can be accomplished through the linearization of all of the elements of the Maglev system. The transfer functions of the aforementioned components, coupled with the PID controller, are presented in Fig.2. Essentially, the controlled Maglev system operates based on error detection. The difference between the reference position and actual position is known as positional error e(t). Subsequently, the PID controller intervenes to regulate this error, enhancing the dynamic response and mitigating steadystate error. The general form of this PID controller is expressed as follows [26]:

$$u(t) = K_p \left(e(t) + \frac{1}{T_i} \int_0^t e(\tau) d\tau \right) + T_d \frac{\partial e(t)}{\partial t} \quad (18)$$

where

u(t): This is the control signal or the output of the PID controller that is applied as the input to the system being controlled.

K_p: This is the proportional gain, a tuning parameter that determines how much the controller responds to the current error.

Ti: This is the integral time or reset time, another tuning parameter that determines how aggressively the controller eliminates the accumulated error over time.

Td: This is the derivative time or rate time, yet another tuning parameter that determines how much the controller anticipates future error based on the rate of change of the error.

e(t): This is the error signal, which is the difference between the desired reference point and the actual output of the plant being controlled.

Together, these parameters and the error signal allow the PID controller to adjust the control output in order to minimize the error and maintain the system at or near the desired setpoint. The specific values of K_p, T_i, and T_d are typically determined through a tuning process to achieve the desired control performance for a given system.

2. **Model Predictive Control (MPC) Design:** This article describes how to create a linear MPC to increase the precision of a Maglev system's control design. Fig.3 depicts the fundamental block diagram of the MPC. Following is a representation of the linear state-space model (discretetime) of the Maglev system:

$$x(\tau+1) = \mathcal{A}_p x(\tau) + \mathcal{B}_p u_p(\tau),$$
$$y(\tau) = \mathcal{C}_p x(\tau) + \mathcal{D}_p u_p(\tau), \quad (19)$$

where x (τ) is a representation of the state vector at instant τ th . Similar to this, at the τ th instant, y (τ) and up (τ) represent output and control input of Maglev, respectively. A MPC has a built-in model that predict the expected plant behavior over a given prediction horizon, or N_p. The optimal control problem is online solved in MPC to identify the control input. The projected output relies on the presumed input trajectory up (τ + j |τ) for j = 0, 1, ..., N_p − 1. The core idea is to select the input that yields the most accurate predictions [14]. In Fig.4, you can see the fundamental concept of linear MPC, where N_p represents the prediction horizon, and N_c is the control horizon. At each time step k, MPC forecasts future outputs over a predefined horizon, N_p. These predicted outputs y (τ + j |τ) for j = 0, 1, ..., N_p − 1, depend not only on past outputs and control inputs but also on future control signals up (τ + j |τ) for j = 0, 1, ..., N_p − 1.

If the relationship between input and output stays linear over the specified time-frame, we can treat the optimization problem as a linear-quadratic one. Here's how the state variables within the prediction horizon are calculated:

$$\begin{aligned}\hat{x}(\tau+2|\tau) &= \mathcal{A}_p(\tau+1|\tau)\,\hat{x}(\tau+1|\tau) \\ &\quad +\mathcal{B}_p(\tau+1|\tau)\,\hat{u_p}(\tau+1|\tau)\end{aligned} \quad (20)$$

(20) can be represented as:

$$\begin{aligned}\hat{x}(\tau+2|\tau) &= \mathcal{A}_p(\tau+1|\tau)\,\mathcal{A}_p(\tau|\tau)\,x(\tau) \\ &\quad +\mathcal{A}_p(\tau+1|\tau)\,\mathcal{B}_p(\tau|\tau)\,\hat{u_p}(\tau|\tau) \\ &\quad +\mathcal{B}_p(\tau+1|\tau)\,\hat{u_p}(\tau+1|\tau),\end{aligned}$$
$$\vdots$$
$$\begin{aligned}\hat{x}(\tau+N_p|\tau) &= \mathcal{A}_p(\tau+N_p-1|\tau)\,\hat{x}(\tau+N_p-1|\tau) \\ &\quad +\mathcal{B}_p(\tau+N_p-1|\tau)\,\hat{u_p}(\tau+N_p-1|\tau)\end{aligned} \quad (21)$$

The control inputs undergo adjustments within the control horizon interval, after which they remain constant.

$$\begin{aligned}\hat{u_p}(\tau+j|\tau) &= \hat{u_p}(\tau+N_c-1|\tau), \\ &\quad N_c \le j \le N_p-1.\end{aligned} \quad (22)$$

The connection between the inputs and the rate of change of inputs is as follows.

$$\hat{u_p}(\tau + j\,|\tau) = u_p(\tau - 1) + \sum_{j=0}^{N_c-1} \Delta\hat{u_{p_i^{\vec{}}}}(\tau + j\,|\tau) \quad j = 0, 1, ..., N_c - 1. \tag{23}$$

By substituting equation (23) into equation (22), the state variable model can be represented as:

$$X(\tau) = \mathcal{Z}_{\mathcal{A}_p}(\tau)\, x(\tau) + \mathcal{Z}_{\mathcal{B}_p}(\tau)\, u_p(\tau - 1) + \mathcal{Z}_{U_p}(\tau)\, \Delta U_p(\tau), \tag{24}$$

where $X(\tau) = \begin{bmatrix} \hat{x}(\tau + 1\,|\tau) \\ \hat{x}(\tau + 2\,|\tau) \\ \vdots \\ \hat{x}(\tau + N_p\,|\tau) \end{bmatrix}$; $\mathcal{Z}_{\mathcal{B}_p}(\tau) = \begin{bmatrix} \mathcal{Z}_{1,1}(\tau) \\ \mathcal{Z}_{2,1}(\tau) \\ \vdots \\ \mathcal{Z}_{N_p,1}(\tau) \end{bmatrix}$;

$$\mathcal{Z}_{\mathcal{A}_p}(\tau) = \begin{bmatrix} \mathcal{A}_p(\tau\,|\tau) \\ \mathcal{A}_p(\tau + 1\,|\tau\,|\tau)\, \mathcal{A}_p(\tau\,|\tau) \\ \vdots \\ \prod_{j=1}^{N_p} \mathcal{A}_p(\tau + N_p - j\,|\tau) \end{bmatrix},$$

$$S_{U_p}(\tau) = \begin{bmatrix} \mathcal{Z}_{1,1}(\tau) & 0 & \cdots & 0 \\ \mathcal{Z}_{2,1}(\tau) & \mathcal{Z}_{2,2}(\tau) & \cdots & 0 \\ \vdots & \vdots & \ddots & \vdots \\ \mathcal{Z}_{N_p,1}(\tau) & \mathcal{Z}_{N_p,1}(\tau) & \cdots & \mathcal{Z}_{N_p,N_p}(\tau) \end{bmatrix}; \text{ and}$$

$$\Delta U_p(\tau) = \begin{bmatrix} \Delta\hat{u_p}(\tau\,|\tau) \\ \Delta\hat{u_p}(\tau + 1\,|\tau) \\ \vdots \\ \Delta\hat{u_p}(\tau + N_c - 1\,|\tau) \end{bmatrix}.$$

Each elements of $\mathcal{Z}_{\mathcal{A}_p}(\tau)$ and $\mathcal{Z}_{\mathcal{B}_p}(\tau)$ are given as:

$\mathcal{Z}_{1,1}(\tau) = \mathcal{B}_p(\tau\,|\tau)$,

$\mathcal{Z}_{2,1}(\tau) = \mathcal{A}_p(\tau + 1\,|\tau)\, \mathcal{B}_p(\tau\,|\tau) + \mathcal{B}_p(\tau + 1\,|\tau)$,

$\mathcal{Z}_{2,2}(\tau) = \mathcal{B}_p(\tau + 1\,|\tau)$,

$$\mathcal{Z}_{N_p,1}(\tau) = \sum_{l=0}^{N_p-2} \left(\prod_{j=1}^{N_c-1-l} \mathcal{A}_c(\tau + N_p - j\,|\tau) \right) \mathcal{B}_p(\tau + l\,|\tau) + \mathcal{B}_p(\tau + N_p - 1\,|\tau),$$

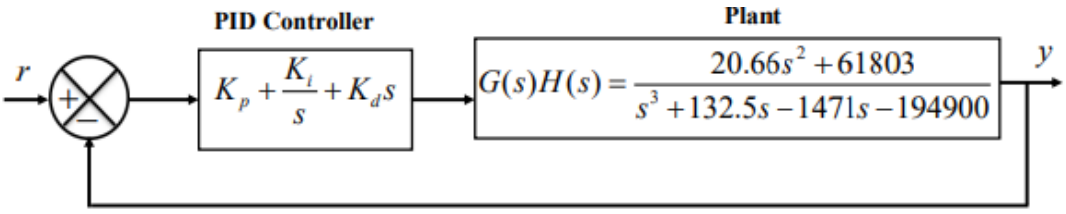

Figure 2: Magnetic levitation system with the PID controller

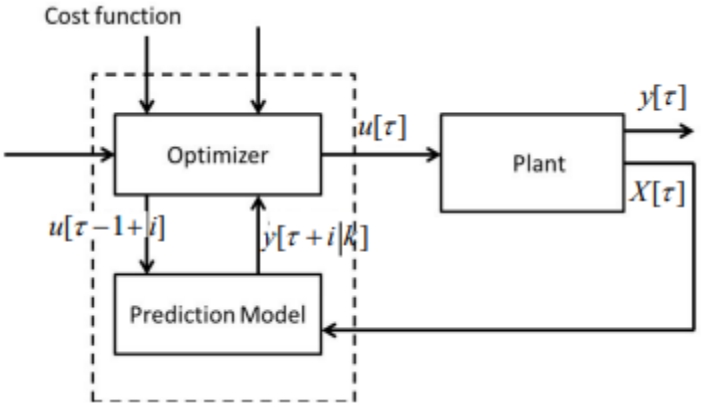

Figure 3: Block diagram for MPC

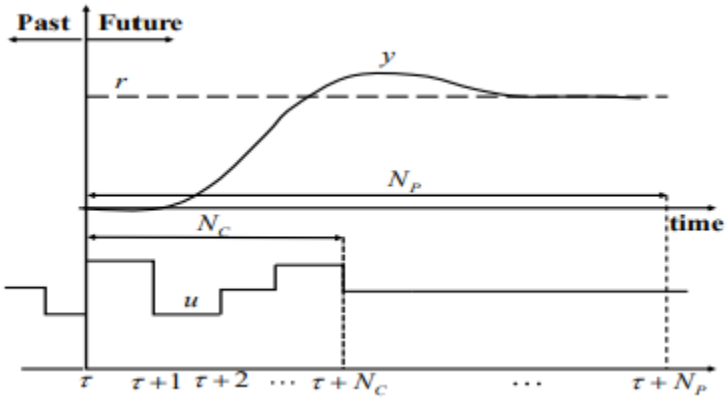

Figure 4: Basic MPC concept

$$\mathcal{Z}_{N_p,N_c}(\tau) = \sum_{l=N_c-1}^{N_p-2} \left(\prod_{j=1}^{N_p-1-l} \mathcal{A}_p(\tau + N_p - j\,|\tau) \right) \mathcal{B}_p(\tau + l\,|\tau) + \mathcal{B}_p(\tau + N_p - 1\,|\tau).$$

The predicted system output can be defined as:

$$Y(\tau) = ZC_pX(\tau), \qquad (25)$$

where

$$Y(\tau) = \begin{bmatrix} \hat{y}(\tau+1|\tau) \\ \hat{y}(\tau+2|\tau) \\ \vdots \\ \hat{y}(\tau+N_p|\tau) \end{bmatrix};$$

$$\mathcal{Z}_{\mathcal{C}_p}(\tau) = \begin{bmatrix} \mathcal{C}_p(\tau+1|\tau) & \cdots & 0 \\ 0 & \cdots & \vdots \\ \vdots & \ddots & \vdots \\ 0 & \cdots & \mathcal{C}_p(\tau+N_p|\tau) \end{bmatrix}$$

Furthermore, by substituting (24) into (25), the output equation rearranged as follows.

$$\begin{aligned} Y(\tau) &= \mathcal{Z}_{\mathcal{C}_p}(\tau)\mathcal{Z}_{\mathcal{A}_p}(\tau)x(\tau) + \mathcal{Z}_{\mathcal{C}_p}(\tau)\mathcal{Z}_{\mathcal{B}_p}(\tau)u_p(\tau-1) \\ &\quad + \mathcal{Z}_{\mathcal{C}_p}(\tau)\mathcal{Z}_{U_p}(\tau)\Delta u_p(\tau). \end{aligned} \tag{26}$$

3. **Objective function and constrains:** By minimizing the specified objective or cost function over the prediction horizon N p, we can determine the optimal input for the magnetic levitation system.

$$\begin{aligned} J(\tau) &= \sum_{j=1}^{N_p} e(\tau+j)^T \delta(j)\, e(\tau+j) \\ &\quad + \sum_{j=1}^{N_c} [\Delta\hat{u_p}(\tau+j-1)]^T \lambda(j) [\Delta\hat{u_p}(\tau+j-1)], \end{aligned} \tag{27}$$

where e (τ + j) = [r (τ + j) − yˆ(τ + j |τ)]. The constraints are as follows:

$$y_{\min} \le \hat{y}(\tau+j|\tau) \le y_{\max}, \qquad j = 1, 2, ..., N_{p,},$$

$$u_{p_{\min}} \le \hat{u_p}(\tau+j-1|\tau) \le u_{p_{\max}}, \qquad j = 1, 2, ..., N_{c,},$$

$$\Delta u_{p_{\min}} \le \Delta\hat{u_p}(\tau+j-1|\tau) \le \Delta u_{p_{\max}}, j = 1, 2, ..., N_{c,},$$

In this context, r symbolizes the future inputs of the system, δ(j) stands for the error weighting matrix, and λ (j) signifies the control weighting matrix. Furthermore, the cost function can be articulated as follows:

$$J(\tau) = E(\tau)^T Q E(\tau) + \Delta U_p{}^T(\tau) R \Delta U_p(\tau), \tag{28}$$

where

$$E(\tau) = [\mathcal{Z}_r(\tau) - Y(\tau)];\ \mathcal{Z}_r(\tau) = \begin{bmatrix} r(\tau+1) \\ r(\tau+2) \\ \vdots \\ r(\tau+N_p) \end{bmatrix};$$

$$Q = \begin{bmatrix} \delta(1) & 0 & \cdots & 0 \\ 0 & \delta(1) & \cdots & 0 \\ \vdots & \vdots & \ddots & \vdots \\ 0 & 0 & \cdots & \delta(N_p) \end{bmatrix};$$

$$R = \begin{bmatrix} \lambda(1) & 0 & \cdots & 0 \\ 0 & \lambda(1) & \cdots & 0 \\ \vdots & \vdots & \ddots & \vdots \\ 0 & 0 & \cdots & \lambda(N_c) \end{bmatrix}.$$

Table 2: Controller parameters

Controller	Parameter	Value
MPC	N_p	20
	N_c	10
	$\delta(j)$	$\begin{bmatrix} 1 & 0 \\ 0 & 5 \end{bmatrix}$
	$\lambda(j)$	$0.002I_{2\times2}$
	T_s	$0.01s$
	u_min	$-2.5v$
	u_max	$2.5v$
PID	K_p	10
	K_i	4
	K_d	0.2

The linear quadratic function can be derived by substituting equation (26) into equation (28) as follows:

$$\begin{aligned} J(\tau) &= \frac{1}{2}\Delta U_p{}^T(\tau) H(\tau) \Delta U_p(\tau) \\ &\quad + \Delta U_p{}^T(\tau) G(\tau) + c(\tau), \end{aligned} \tag{29}$$

where

$$\begin{aligned} H(\tau) &= 2\left(\mathcal{Z}_{U_p}^T(\tau)\,\mathcal{Z}_{C_p}^T(\tau)\,Q\mathcal{Z}_{C_p}(\tau)\,\mathcal{Z}_{U_p}(\tau)+R\right), \\ G(\tau) &= -2\mathcal{Z}_{U_p}^T(\tau)\,\mathcal{Z}_{C_p}^T(\tau)\,QE(\tau), \\ c(\tau) &= E^T(\tau)\,QE(\tau), \\ E(\tau) &= \mathcal{Z}_r(\tau)-\mathcal{Z}_{C_p}(\tau)\,\mathcal{Z}_{\mathcal{A}_p}(\tau)\,x(\tau) \\ &\quad -\mathcal{Z}_{C_p}(\tau)\,\mathcal{Z}_{\mathcal{B}_p}(\tau)\,u_p(\tau-1). \end{aligned}$$

To maintain control stability during each sampling period, the optimization problem for the proposed adaptive MPC includes additional input and output constraints.

IV. RESULTS AND DISCUSSION

In this research, a linearized model of the magnetic levitation system was created using the MATLAB Simulink platform, with parameters set to their nominal values as detailed in TABLE I. The initial state variable value for the system was set to zero. Controller parameters for both the proposed MPC algorithm and the PID controller are provided in TABLE II. The controller's performance was assessed through simulations using two different reference signals.

Case 1: In this scenario, a desired step input signal with an amplitude of 0.3mm is applied to the Maglev model. Fig.5 provides a simulated comparison between the proposed MPC and the existing PID controller [1] for step signal tracking. Additionally, Fig.6 displays the control inputs generated by both the proposed MPC and the existing PID controller. These results illustrate that the proposed MPC surpasses the performance of the existing control algorithms in terms of regulation response, convergence speed, and minimal steadystate error [1].

Case 2: In Figure 7, the Maglev system's response to a square wave reference signal with an amplitude of 0.3mm and a period of 50s is shown. This square wave input is used to evaluate the controller's ability to handle abrupt changes in the input signal direction. As demonstrated in Figure 8, the MPC exhibits significantly improved performance compared to the existing PID controller [1].

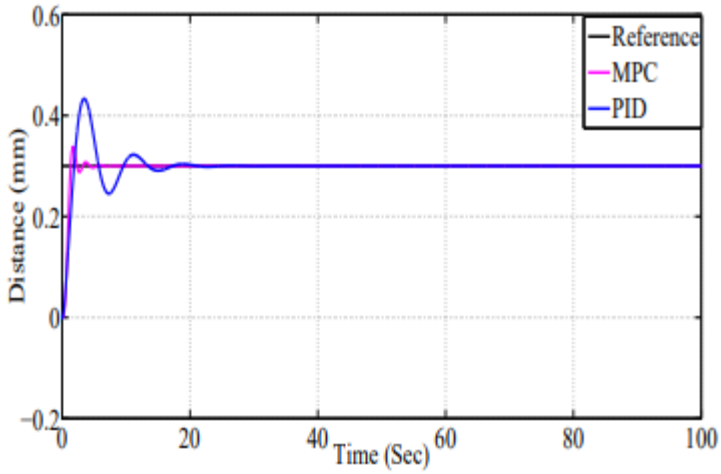

Figure 5: Step response

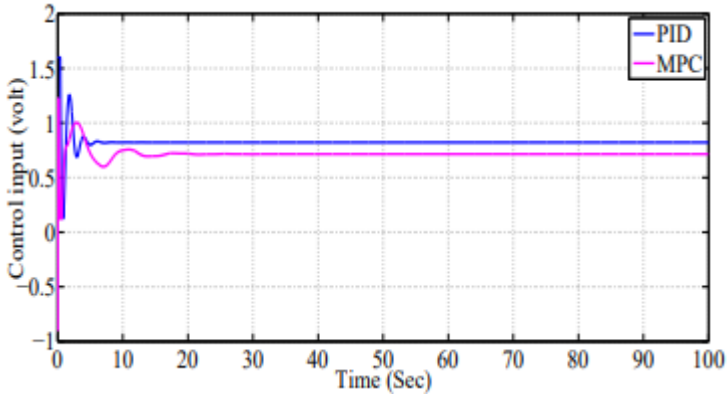

Figure 6: Control input for step signal

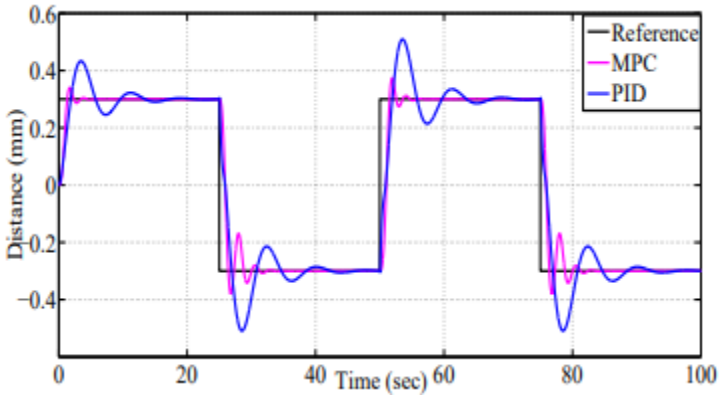

Figure 7: Square response

Table III tabulates the comparative tracking results of the proposed MPC with the existing controllers developed in [1]. As can be observed from Table III, the proposed MPC gives 44.70%, 62.25% and 65.92% lower RMSE, ISE and IAE values as compared to PID

[1] control algorithm for case 1. While for case2, it gives 4.04%, 7.88% and 51.02% lower RMSE, ISE and IAE values as compared to PID [1] respectively. Furthermore, Table III shows that the suggested MPC is more energy-efficient than the controllers developed in [1]. The proposed MPC provides 11.2% lower kuk2 value for case 1 and 35.76%, lower kuk2 value for case 2 of PID [1] controller, respectively.

Table 3: Performance analysis for both the cases

Control Action		Performance Specification					
		M_p	RMSE	ISE	IAE	TV	$\|u\|_2$
Case 1	MPC	12.49	0.094	62.07	209.8	3.49	201.9
	PID [1]	44.4	0.170	168.9	855.1	4.7	227.4
Case 2	MPC	24.66	0.095	906.7	$2.4e^{03}$	30.8	323.8
	PID [1]	69.7	0.09	984.3	$4.9e^{03}$	402.5	504.05

V. CONCLUSION

The paper presents a linear model predictive control (MPC) algorithm developed for a highly nonlinear Maglev system. To ensure a fair comparison, an existing PID control algorithm with parameters matching those in [1] has been implemented. The efficacy of the proposed control algorithm is validated through simulations using three different reference signals. The simulation results demonstrate that the proposed controller outperforms the existing control algorithm [1] in terms of achieving the desired trajectory tracking.

REFERENCES

[1] M. H. Yaseen and H. J. Abd, "Modeling and control for a magnetic levitation system based on simlab platform in real time," *Results in Physics*, vol. 8, pp. 153–159, 2018.
[2] S. Yadav, S. Verma, and S. Nagar, "Optimized pid controller for magnetic levitation system," *Ifac-PapersOnLine*, vol. 49, no. 1, pp. 778– 782, 2016.
[3] A. Winursito and G. Pratama, "Lqr state feedback controller with precompensator for magnetic levitation system," in *Journal of Physics: Conference Series*, vol. 2111, no. 1. IOP Publishing, 2021, p. 012004.
[4] S. K. Pradhan and B. Subudhi, "Nonlinear control of a magnetic levitation system using a new input-output feedback linearization," *IFAC-PapersOnLine*, vol. 49, no. 1, pp. 332–336, 2016.
[5] Z.-J. Yang and M. Minashima, "Robust nonlinear control of a feedback linearizable voltage-controlled magnetic levitation system," *IEEJ Trans- actions on Electronics, Information and Systems*, vol. 121, no. 7, pp. 1203–1211, 2001.
[6] A. S. Malik, I. Ahmad, A. U. Rahman, and Y. Islam, "Integral back- stepping and synergetic control of magnetic levitation system," *IEEE Access*, vol. 7, pp. 173 230–173 239, 2019.
[7] Z.-J. Yang, K. Kunitoshi, S. Kanae, and K. Wada, "Adaptive robust output-feedback control of a magnetic levitation system by k-filter approach," *IEEE Transactions on Industrial Electronics*, vol. 55, no. 1,pp. 390–399, 2008.
[8] R. H. Milani, H. Zarabadipour, and R. Shahnazi, "An adaptive robust controller for time delay maglev transportation systems," *Communica- tions in Nonlinear Science and Numerical Simulation*, vol. 17, no. 12, pp. 4792–4801, 2012.
[9] H.-S. Lee, J. Back, and C.-S. Kim, "Disturbance observer-based robust controller for a multiple-electromagnets actuator," *IEEE Transactions on Industrial Electronics*, 2023.
[10] J. Xu, Y. Sun, D. Gao, W. Ma, S. Luo, and Q. Qian, "Dynamic modeling and adaptive sliding mode control for a maglev train system based on a magnetic flux observer," *Ieee Access*, vol. 6, pp. 31 571–31 579, 2018.
[11] Y.-G. Sun, J.-Q. Xu, C. Chen, and G.-B. Lin, "Fuzzy h infinity robust control for magnetic levitation

system of maglev vehicles based on ts fuzzy model: Design and experiments," *Journal of Intelligent & Fuzzy Systems*, vol. 36, no. 2, pp. 911–922, 2019.

[12] R.-J. Wai, M.-W. Chen, and J.-X. Yao, "Observer-based adaptive fuzzy- neural-network control for hybrid maglev transportation system," *Neu- rocomputing*, vol. 175, pp. 10–24, 2016.

[13] J. Mao and C. G. Cassandras, "Optimal control of multilayer discrete event systems with real-time constraint guarantees," *IEEE Transactions on Systems, Man, and Cybernetics: Systems*, vol. 44, no. 10, pp. 1425– 1434, 2014.

[14] L. Dutta and D. Kumar Das, "Adaptive model predictive control design using multiple model second level adaptation for parameter estimation of two-degree freedom of helicopter model," *International Journal of Robust and Nonlinear Control*, vol. 31, no. 8, pp. 3248–3278, 2021.

[15] W. Hu, Y. Zhou, Z. Zhang, and H. Fujita, "Model predictive control for hybrid levitation systems of maglev trains with state constraints," *IEEE Transactions on Vehicular Technology*, vol. 70, no. 10, pp. 9972–9985, 2021.

[16] L. Dutta and D. K. Das, "Nonlinear disturbance observer-based adaptive nonlinear model predictive control design for a class of nonlinear mimo system," *International Journal of Systems Science*, vol. 53, no. 9, pp. 2010–2031, 2022.

[17] D. Q. Mayne, J. B. Rawlings, C. V. Rao, and P. O. Scokaert, "Con- strained model predictive control: Stability and optimality," *Automatica*, vol. 36, no. 6, pp. 789–814, 2000.

[18] G. P. Incremona, A. Ferrara, and L. Magni, "Mpc for robot manipulators with integral sliding modes generation," *IEEE/ASME Transactions on Mechatronics*, vol. 22, no. 3, pp. 1299–1307, 2017.

[19] L. Dutta and D. Kumar Das, "Nonlinear disturbance observer based multiple-model adaptive explicit model predictive control for nonlinear mimo system," *International Journal of Robust and Nonlinear Control*, vol. 33, no. 11, pp. 5934–5955, 2023.

[20] D. Tavernini, M. Metzler, P. Gruber, and A. Sorniotti, "Explicit nonlinear model predictive control for electric vehicle traction control," *IEEE Transactions on Control Systems Technology*, vol. 27, no. 4, pp. 1438– 1451, 2018.

[21] M. Santos, R. Galvao, and T. Yoneyama, "Robust model predictive control for a magnetic levitation system employing linear matrix in- equalities," in *ABCM Symposium Series in Mechatronics*, vol. 4, 2010,pp. 147–155.

[22] Y. Qin, H. Peng, W. Ruan, J. Wu, and J. Gao, "A modeling and control approach to magnetic levitation system based on state-dependent arx model," *Journal of Process Control*, vol. 24, no. 1, pp. 93–112, 2014.

[23] M. Klaucˇo, M. Kaluz, and M. Kvasnica, "Real-time implementation of an explicit mpc-based reference governor for control of a magnetic levitation system," *Control Engineering Practice*, vol. 60, pp. 99–105, 2017.

[24] L. Dutta and D. K. Das, "A linear model predictive control design for magnetic levitation system," in *2020 International Conference on Computational Performance Evaluation (ComPE)*. IEEE, 2020, pp. 039–043.

[25] T. Ba¨chle, S. Hentzelt, and K. Graichen, "Nonlinear model predictive control of a magnetic levitation system," *Control Engineering Practice*, vol. 21, no. 9, pp. 1250–1258, 2013.

[26] G. Gurumurthy and D. K. Das, "A semi-analytical approach to design a fractional order proportional-integral-derivative (fopid) controller for a tito coupled tank system," in *2019 IEEE Asia Pacific Conference on Circuits and Systems (APCCAS)*. IEEE, 2019, pp. 233–236.

